Predicting the State of the Southern Oscillation Using Principal Oscillation Pattern Analysis

JIN-SONG XU AND HANS VON STORCH

Max Planck Institut für Meteorologie, Hamburg, Federal Republic of Germany

(Manuscript received 21 July 1989, in final form 1 June 1990)

ABSTRACT

Principal oscillation pattern (POP) analysis is a diagnostic technique for deriving the space–time characteristics of a dataset objectively. A multiyear dataset of monthly mean sea level pressure (SLP) in the area 15°S to 40°S is examined with the POP technique. In the low-frequency band one physically significant pair of patterns is identified, which is clearly associated with the Southern Oscillation (SO).

According to the POP analysis, the SO may be described as a damped oscillatory sequence of patterns $\cdots \rightarrow \mathbf{P}^1 \rightarrow \mathbf{P}^2 \rightarrow -\mathbf{P}^1 \rightarrow -\mathbf{P}^2 \rightarrow \mathbf{P}^1 \rightarrow \cdots$ having a time scale of two to three years. The first pattern, $\mathbf{P}^1$, representative of the "peak" phase of ENSO, exhibits a dipole with anomalies of opposite sign over the central and eastern Pacific and over the Indian Ocean/Australian sector. The second, $\mathbf{P}^2$, pattern is dominated by an anomaly in the SPCZ region and describes an intermediate, or "onset" phase.

The time coefficients of the two patterns, $\mathbf{P}_1$ and $\mathbf{P}_2$, may be interpreted as a bivariate index of the SO. Generalizing the original diagnostic concept, the POP framework is used to predict this index and the traditional univariate SO index.

The POP prediction scheme is tested in a series of hindcast experiments. The scheme turns out to be skillful for a lead time of two to three seasons. In terms of a correlation skill score, the POP model is better than persistence and a conventional ARMA model in hindcasting the traditional SO index.

1. Introduction

In the last decade a large body of observational literature on the appearance and low-frequency evolution of the El Niño/Southern Oscillation (ENSO) has been published. For example, Rasmusson and Carpenter (1982) composited the development of sea surface temperatures (SST) and wind anomalies during warm events; van Loon and colleagues, in a series of papers, examined SO-related variations of various meteorological parameters (van Loon and Madden 1981; van Loon 1984; van Loon and Shea 1985, 1987; van Loon and Labitzke 1987)—in particular, sea level pressure in the Southern Hemisphere. Ropelewski and Halpert (1987) investigated the global precipitation variations associated with SO.

Originally, the Southern Oscillation was primarily viewed as a "standing" feature (Trenberth and Shea 1988), which could be monitored by a variety of (mostly equivalent) indices (e.g., Wright 1984). With the advent of longer time series of gridded tropical data, it became apparent that ENSO should be regarded as a propagating phenomenon (Barnett 1985, 1988; Storch et al. 1989, 1990). However, there still exists no agreement within the scientific community about the physical process responsible for the occurrence and propagation of ENSO. One theory suggests that equatorial ocean waves are a crucial ingredient (Suarez and Schopf 1988; Cane and Zebiak 1985), while others propose that land–atmosphere or ocean–atmosphere interactions (Barnett et al. 1989; van Loon and Shea 1985, 1987) are essential for understanding ENSO.

A few groups are now actively making operational predictions of the state of ENSO (e.g., Barnett et al. 1988). Most of the schemes (Inoue and O'Brien 1974; Cane et al. 1986; White et al. 1987) are based on the notion of tropical Pacific wave propagation, while Barnett (1984) and Graham et al. (1987) exploit the propagation of atmospheric signals. The forecast schemes are methodologically quite different, ranging from statistical models to dynamical ones; but they all are based on the idea of a regular low-frequency evolution of anomalies.

Clearly, the problem of ENSO prediction is equivalent to the problem of recognizing and understanding such quasi-cyclic large-scale behavior. Principal oscillation pattern (POP) analysis, recently introduced by Hasselmann (1988) and Storch et al. (1988), is a technique specifically designed to identify regularly developing space–time patterns. In the present paper, the POP technique is used not only as a diagnostic tool but also as a predictive one. It is applied specifically to the "atmospheric" ENSO hypothesis of van Loon and Shea (1985, 1987), who suggested that the South Pa-

Corresponding author address: Dr. Hans von Storch, Max Planck Institut für Meteorologie, Bundestrasse 55, D 2000 Hamburg 13, FR Germany.

cific convergence zone (SPCZ) and its interaction with the underlying ocean might be instrumental in the ENSO cycle. Because it is possible to monitor both the Southern Oscillation index (SOI) and the state of the SPCZ in the routinely available Southern Hemisphere sea level pressure (15°–40°S) analysis, we have used this dataset in the present study.

The paper is organized as follows: In section 2, the POP analysis and POP prediction technique are presented. The data are described in section 3a, and the results of the POP analysis are presented in section 3b. In section 4, the POP technique's capability to forecast the state of the SO is discussed with the aid of case studies and an ensemble measure of skill obtained in a series of hindcast experiments. Finally, a discussion of the results is given in section 5.

2. Concepts of POP analysis and POP prediction

a. POP analysis

Principal oscillation pattern analysis is a technique for extracting regularly developing (e.g., oscillating or standing) spatial patterns from a multicomponent system whose dynamics are unknown or too complex to be easily described (Storch et al. 1988). Conceptually, POP analysis represents a simplification of principal interaction pattern analysis (Hasselmann 1988). Alternatively, POP analysis may be thought of as a normal mode analysis using an estimated system matrix. In this section we describe this approach briefly. More details are given by Storch et al. (1988, 1990).

To focus on specific time scales, the vector time series to be analyzed is filtered in time and space, retaining variability only on the temporal and spatial scales of interest. The filtered time series, $\mathbf{x}(t)$, is then assumed to be generated by a first-order multivariate autoregressive process:

$$\mathbf{x}(t+1) = A\mathbf{x}(t) + \text{forcing}. \tag{1}$$

If the forcing in (1) is uncorrelated with $\mathbf{x}(t)$, an estimate of the matrix A may be obtained in two different ways: one way is to multiply (1) from the right with the transpose of $\mathbf{x}(t)$ and to take expectations. The other way is to find a matrix A that minimizes $\{[\mathbf{x}(t+1) - A\mathbf{x}(t) - \text{forcing}]^2\}$. In both cases the result is $A = C_1 \cdot C_0^{-1}$ with C_1 and C_0 denoting the lag-1 and lag-0 covariance matrices of $\mathbf{x}(t)$. The matrices C_1 and C_0 are estimated in the conventional manner.

Generally, the matrix A is not symmetric, and thus its eigenvectors $\mathbf{P}$ and eigenvalues λ are not all real. Some may occur in pairs of conjugate complex eigenvectors, $\mathbf{P}^1 \pm i\mathbf{P}^2$, and eigenvalues, $\lambda^1 \pm i\lambda^2$. The (real or complex) eigenvectors are called POPs of the time series $\mathbf{x}(t)$. In most cases, the eigenvectors are linearly independent so that the state $\mathbf{x}(t)$ may uniquely be written as

$$\mathbf{x}(t) = \underbrace{\sum_j z_j(t)\mathbf{P}_j}_{\substack{\text{all real}\\ \text{POPs}}} + \underbrace{\sum_j (z_j^1(t)\mathbf{P}_j^1 + z_j^2(t)\mathbf{P}_j^2)}_{\substack{\text{all complex}\\ \text{POPs}}} + \text{forcing} \tag{2}$$

with real-time coefficients $z(t)$ for real POPs and complex time coefficients $z(t)$ with real part $z^1(t)$ and imaginary part $z^2(t)$ for complex POPs. The coefficients may be obtained by taking the dot product of the vector $\mathbf{x}(t)$ and the adjoint eigenvector.

The time evolution of the coefficients satisfies, for real patterns, the equation

$$z(t_0 + t) = \lambda^t z(t_0) + \text{forcing} \tag{3}$$

and for complex patterns,

$$[z^1(t_0+t) + iz^2(t_0+t)] = (|\lambda| e^{-2\pi i/T})^t [z^1(t_0) + iz^2(t_0)] + \text{forcing}. \tag{4}$$

For complex patterns the complex eigenvalues define an e-folding time τ and rotation period T. Because of the particular form of (3) and (4), the real valued POPs are called standing patterns and the complex valued POPs oscillatory patterns. An oscillatory pattern often describes a feature that migrates in space. This is particularly true if the real part $\mathbf{P}^1$ and the imaginary part $\mathbf{P}^2$ are spatially in quadrature.

The error, $\mathbf{e}(t) = \mathbf{x}(t) - z(t)\cdot\mathbf{P}$ or $\mathbf{e}(t) = \mathbf{x}(t) - z^1(t)\cdot\mathbf{P}^1 - z^2(t)\cdot\mathbf{P}^2$, in reproducing $\mathbf{x}(t)$ using only one standing real POP $\mathbf{P}$ or one oscillatory complex POP $\mathbf{P}^1 + i\mathbf{P}^2$ may be conveniently measured by the skill parameter

$$S^r = 1 - \frac{\langle \mathbf{e}^2 \rangle}{\langle \mathbf{x}^2 \rangle} \tag{5}$$

where $\langle\ \rangle$ denotes expectation. $S^r = 0$ indicates that the POP model has no skill, whereas $S^r = 1$ indicates perfect skill.

After having identified a certain POP in the "key variable" $\mathbf{x}(t)$, it is often desirable to describe the signal in terms of other simultaneously observed variables $\mathbf{v}(t)$; e.g., SST. To do this, we use "associated correlation patterns." In the case of an oscillatory mode these patterns, denoted by $\mathbf{q}_v{}^1$ and $\mathbf{q}_v{}^2$, are defined to minimize

$$\left\langle \left\| \mathbf{v}(t) - \frac{z^1(t)}{\sigma^1}\mathbf{q}_v{}^1 - \frac{z^2(t)}{\sigma^2}\mathbf{q}_v{}^2 \right\|^2 \right\rangle \tag{6}$$

where $\|\ \|$ denotes a quadratic norm. The coefficients $z^1(t)$ and $z^2(t)$ of the *key variable* $\mathbf{x}$ are divided by their standard deviations, σ^1 and σ^2, in order to convert the patterns into the same units as the field $\mathbf{v}$.

In the case of oscillatory patterns, the POP model can be interpreted as the system's tendency to generate a damped oscillation with parallel evolutions of $\mathbf{x}(t)$ and $\mathbf{v}(t)$ as follows:

for $\mathbf{x}(t)$: $\ldots \rightarrow \mathbf{P}^1 \rightarrow \mathbf{P}^2 \rightarrow -\mathbf{P}^1 \rightarrow -\mathbf{P}^2 \rightarrow \mathbf{P}^1 \rightarrow \ldots$

for $\mathbf{v}(t)$: $\ldots \rightarrow \mathbf{q}_v{}^1 \rightarrow \mathbf{q}_v{}^2 \rightarrow -\mathbf{q}_v{}^1 \rightarrow -\mathbf{q}_v{}^2 \rightarrow \mathbf{q}_v{}^2 \rightarrow \ldots$.

b. Comparisons with other empirical orthogonal functions

More traditionally the concept of empirical orthogonal functions (e.g., Preisendorfer 1988) has been used to infer the space–time variability in a multicomponent time series. The EOF analysis is designed to yield an optimal representation of the covariance structure of fields. Only in very specific cases do EOFs represent dynamical modes of the investigated system. In the case of conventional EOFs, simultaneous covariances are considered and the spatial patterns represent standing features. With extended EOFs lagged covariances are also taken into account so that it is possible to describe time-dependent spatial patterns. In the complex EOF analysis, the eigenvalues and eigenvectors of the cross-spectral matrix averaged over a certain frequency band are derived. The resulting complex eigenvectors may be used to describe oscillatory behavior in space. In all cases, the EOF analysis leads to patterns that maximize variances. The eigenvalues represent the amount of variance explained by the patterns. The characteristic time scales have to be inferred by cross-spectral analysis of the EOF coefficients.

The POPs are based on a different notion. POPs represent the normal modes of a fitted linear stochastic process. As such, the POPs do not maximize the explained variance but satisfy a dynamical constraint, namely $A\mathbf{P} = \lambda\mathbf{P}$. The eigenvalue λ, being in general complex, represents two characteristic times: the rotation period and a damping time. In contrast to EOFs, the POPs do not form a set of orthogonal patterns, so that the POP coefficients are not given as the dot product of the patterns with the field to be analyzed but as the dot product of this field with the adjoint patterns. Also the POP coefficients are not necessarily independent, as the EOF coefficients are. Dynamically this lack of independence is not disadvantageous: there is no a priori reason why different processes, identified by POPs, should be statistically independent. Another difference from EOFs is that the POP analysis yields no information about the amount of variance connected with individual POPs. The explained variance has to be calculated explicitly from the data.

There are two different ways to estimate the POPs. One way, originally proposed by Hasselmann (1988), consists of anticipating the existence of a linear first-order model and fitting the complex number λ and the patterns $\mathbf{P}$ simultaneously to the data in a least-square sense. The other way, suggested by Storch et al. (1988), is to estimate the matrix A from the data and to use the eigenvalues and eigenvectors of this estimated A as characteristic numbers and POPs. The eigenvectors depend nonlinearly on the matrix. Therefore the dynamical model for the POP coefficients, $z(t_0 + t) = \lambda^t z(t_0) +$ forcing, is not strictly a least-square fit to the data.

In summary, the main difference between the POP and EOF techniques is that the latter maximizes variances whereas the former explicitly specifies a dynamical model (1). The time evolution of the POPs is therefore easily interpreted, and the original system is reduced to linear interactions of patterns in two-dimensional spaces spanned by (complex) POPs.

c. The POP prediction scheme

For the sake of brevity, we consider only oscillatory, i.e., complex valued, POPs in this section. For standing patterns, the scheme takes a similar form.

Let us assume that a relevant oscillatory POP, $\mathbf{P}^1 + i\mathbf{P}^2$, has been identified. Its state at a certain time t_0 is measured by the complex coefficient $\mathbf{z}(t_0) = z^1(t_0) + iz^2(t_0)$. Its future state, $\mathbf{z}(t_0 + t)$, would be known if the forcing in (4) were known. Obviously, the forcing describes all processes that cannot be treated in the linear scheme (1). Thus the forcing is considered to be unpredictable noise and the future state is predicted from

$$[\hat{z}^1(t_0 + t) + i\hat{z}^2(t_0 + t)] = (|\lambda|e^{-2\pi i/T})^t[z^1(t_0) + iz^2(t_0)], \quad (7)$$

which is obtained from (4) by neglecting the forcing. Thus the prediction problem is reduced to estimating the initial value $\mathbf{z}(t_0)$.

If the raw data are not filtered in time, the estimation is straightforward. First, the data are filtered in space, if necessary, and then the time coefficient is calculated using the adjoint patterns. In the hindcast experiments in this study, however, the data are noisy and have to be smoothed before the initial value is estimated. For this purpose a nonsymmetric time domain filter is applied (see Appendix), which approximates the spectral characteristics of the frequency domain filter used in the POP analysis.

The time evolution of the process to be described by a complex POP may conveniently be represented in the two-dimensional $\mathbf{z}$-plane. Utilizing (4) or (7), the $z(t)$ trajectory normally rotates clockwise around the origin. Its magnitude may be described by the S-distance, $d(\mathbf{z})$, of $\mathbf{z}(t)$ from the origin:

$$d(\mathbf{z}) = \mathbf{z}' \cdot S^{-1} \cdot \mathbf{z} \quad (8)$$

with S being the covariance matrix ($\langle z^j z^k \rangle$) of $\mathbf{z}$. If $\mathbf{z}$ is normally distributed with zero mean and z^1 and z^2 are independent, the S-distance $d(\mathbf{z})$ is χ^2-distributed. Here $\mathbf{z}(t)$ is considered to be "small" or "very large," if $d(\mathbf{z}) \leq b_1$ or $d(\mathbf{z}) \geq b_2$ for some appropriate numbers

b_1 and b_2. If $\mathbf{z}$ is small, the process described by the POP pair is interpreted as being in a "quiet phase." If $\mathbf{z}$ is not small, the process is "active"; if it is very large, the process is "strongly active."

In this study the SO is divided into three classes of states of equal likelihood: quiet phases, and Warm and Cold phases. The latter two phases comprise the active stage, and the strongest 10% of all states are considered as being strongly active. Therefore the critical values b_1 and b_2 are chosen so that $\text{prob}\{d(\mathbf{z}) \leq b_1\} < 33\%$ and $\text{prob}\{d(\mathbf{z}) \geq b_2\} < 10\%$.

To assess the proposed POP scheme's predictive capabilities, the outcome of a series of hindcast experiments can be compared with a traditional reference, the persistence forecast (Livezey 1987), and a conventional univariate ARMA process (Chu and Katz 1985). To do this, a univariate prediction skill is required:

$$S^p = \frac{\langle O \cdot P_\tau \rangle}{\sqrt{\langle O^2 \rangle \langle P_\tau^2 \rangle}} \tag{9}$$

where $O(t)$ and $P_\tau(t)$ are the observed and, at lag τ, predicted variables. If this variable is perfectly predicted, $S^p = 1$, whereas $S^p = 0$ for a useless prediction. S^p is certainly not the optimal measure with which to compare two sets of hindcasts. In particular, it is not sensitive to systematic errors in the strength of the predicted signal, so that persistence and damped persistence forecasts yield identical skills S^p.

3. The POP analysis

In this section we describe the results of a POP analysis of the Southern Oscillation.

a. Data

The key variable used here is the field of monthly mean SLP in the area from 15°S to 40°S. The data come from two periods: the first extends from January 1951 to December 1958 (South Africa Weather Service), and the second extends from April 1972 to September 1988 (Australian Bureau of Meteorology). We have chosen this dataset since new data for future forecasts are readily available from the routine analyses of the Australian Bureau of Meteorology.

Prior to the analysis, the SLP data were processed as follows:

- The anomaly fields are calculated separately for the two periods 1951–58 and 1972–83 in order to remove long-term trends (Mo and van Loon 1985) and possible inhomogeneities in the datasets.
- At each grid point, the time series are normalized by the local standard deviation. This procedure is necessary because of the considerable difference in variability of midlatitude SLP and subtropical SLP.
- All variance on time scales shorter than 15 months is filtered out, and all variance on time scales greater than 18 months is retained unaltered (see Appendix). The characteristics of the filter have been chosen to focus on the ENSO phenomenon, whose minimum time scale is two years, since an event extends over at least one year.

The time filtering did not take into account the 1959–71 gap between the datasets. This is reasonable when estimating the statistical parameters: The data are noisy, and the sole effect of the sudden 1959/71 jump is to slightly distort the spectral estimates.

- The time-filtered data are projected onto the subspace spanned by the first 9 EOFs, which explains 85% of the total variance. Some experiments were made to determine the optimal number of EOFs to retain. It turned out that the results are stable if at least the first nine EOFs that are used.

The aim of the POP analysis is to identify patterns that describe the Southern Oscillation. Therefore, the low-frequency filtered conventional Southern Oscillation index, Darwin minus Papeete, Tahiti SLP, is used to verify the outcome of the analysis. The SOI is filtered in the same way as the SLP data.

To study the relationship between the "key" variable, namely the subtropical and midlatitude normalized monthly mean SLP, and other variables that contain an ENSO signal, associated correlation patterns are derived for Pacific SST and the zonal component of the equatorial surface wind. The SST data are in the area from 60°N to 40°S and extend from 1972 to 1988, whereas the equatorial zonal wind data are available for the same two periods as the key variable; i.e., from 1951 to 1958 and from 1972 to 1985. No filtering and normalization are performed on these two datasets.

b. Results

One useful oscillatory POP pair was found in the SLP data. Its oscillation period T is about 37 months, and its e-folding time τ is about 47 months. The explained variance S^r of this POP pair is 16% for the entire subtropical Southern Hemisphere SLP time series and 48% for the Southern Oscillation index. The latter number is increased to 73% if the "bad" 1951–58 data are disregarded (see Fig. 1b).

The POP coefficient time series, $z^1(t)$ and $z^2(t)$, are shown in Fig. 1 together with the filtered SOI. In the years of warm events: 1951, 53, 57, 72, 76/77, 82, and 87 (cold events 1955, 73, 75, and 88), when the SOI is minimum (maximum), the coefficient $z^1(t)$ is generally also minimum (maximum) almost simultaneously, and $z^2(t)$ is minimum (maximum) several months later. It seems that the appearance of events is connected to the oscillatory behavior of the two time series. The oscillation period varies between two and three years. The results of cross-spectral analysis (not shown) of the POP coefficients and the SOI substantiate these impressions. The coherences between each two

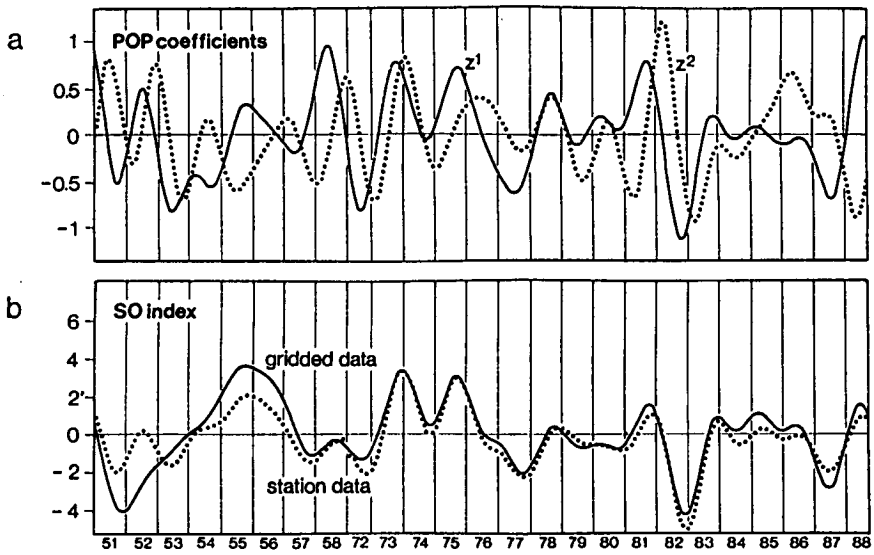

FIG. 1. Time series of a) POP coefficients $z^1(t)$ (heavy) and $z^2(t)$ (dotted). The coefficients are dimensionless. b) Southern oscillation index "Darwin minus Papeete SLP" as derived from station data (solid) and analyzed gridpoint data [dotted; prepared by the South African Weather Service (1951–58) and by the Australian Bureau of Meteorology (1972–88)]. Note the large differences in the 1950s. The curves are time-filtered. Units: mb.

time series, z^1, z^2, and SOI, are high on the time scale of 2–3 years (significantly nonzero at a level of more than 95%). z^1 and z^2 are 90° out-of-phase, with z^1 leading z^2. z^1 leads the SOI by about two months, and z^2 lags the SOI by about seven months. Maximum coherence is obtained for 30 months, indicating that the POP period of 37 months is an overestimation of the oscillation period. The discrepancy between the 37 months derived from the POP analysis and the 30 months inferred from the cross-spectral analysis is due to the fact that both techniques yield estimates of the considered parameter; i.e., both techniques have a certain natural uncertainty.

The patterns are shown in Fig. 2. The $\mathbf{P}^1$ pattern has large positive anomalies over the central and eastern Pacific and negative anomalies over Australia and the Indian Ocean, which are connected with westerly wind anomalies in the eastern tropical Indian Ocean and northerly wind anomalies in the region near the date line. According to the POP model and the oscillatory behavior mentioned above, the $\mathbf{P}^1$ pattern is gradually replaced by the $\mathbf{P}^2$ pattern within a quarter of a period; i.e., after seven to nine months. This replacement appears in space as a smooth eastward migration of the negative $\mathbf{P}^1$ anomaly into the western Pacific. The $\mathbf{P}^2$ anomalies are connected with westerly wind anomalies over the tropical west Pacific. Half a period later the $-\mathbf{P}^1$ pattern is dominant. It is associated with easterly anomalies over the eastern tropical Indian Ocean and southerly anomalies near the date line. At three-quarters of a period ($-\mathbf{P}^2$) there is a center of positive anomalies north of New Zealand, which is connected

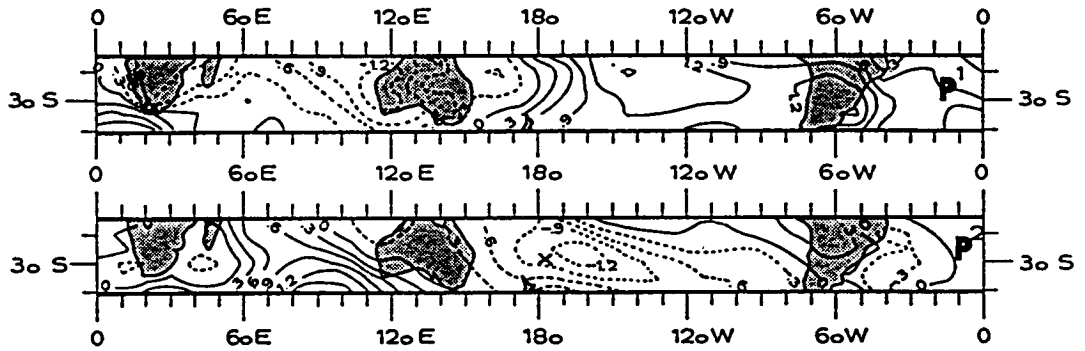

FIG. 2. POP patterns $\mathbf{P}^1$ (bottom) and $\mathbf{P}^2$ (top) of normalized Southern Hemisphere sea level pressure anomalies. The location of Raoul Island, used in section 5a, is marked in $\mathbf{P}^2$.

with easterly anomalies over the tropical west Pacific. After a full period the $\mathbf{P}^1$ pattern reappears.

The associated correlation pattern analysis of SST (Fig. 3a) substantiates the result that the POP obtained here describes the Southern Oscillation. The associated SST pattern $\mathbf{q}^1_{sst}$ (strong negative SST anomalies in the tropical central and east Pacific, positive SST anomalies around Indonesia and in the subtropical northwest and southwest Pacific, and negative SST anomalies in the Indian Ocean) tends to appear together with $\mathbf{P}^1$ (positive SLP anomalies over the east Pacific and negative SLP anomalies over Australia). $\mathbf{P}^1$ represents a negative extreme of the Southern Oscillation and $\mathbf{q}^1_{sst}$ represents a La Niña condition of the ocean. In $\mathbf{q}^2_{sst}$, SST anomalies are weaker than a quarter of a period earlier in $\mathbf{q}^1_{sst}$. Negative anomalies are found in the zonal belt between 5°N and 20°S in the central Pacific, with positive anomalies south and north of this belt. The variance of the unfiltered monthly mean SST anomalies explained by the associated patterns $\mathbf{q}^1_{sst}$ and $\mathbf{q}^2_{sst}$ is about 50% in the central and east Pacific (not shown).

The associated patterns of the zonal component of equatorial surface wind are shown in Fig. 3b. The first pattern, $\mathbf{q}_u{}^1$, shows wind anomalies that are well known to accompany the SST anomalies of $\mathbf{q}^1_{sst}$; namely westerly anomalies over the equatorial east Indian Ocean and easterly anomalies over the central Pacific. According to the POP picture, the development of a warm event begins about a quarter of a period later. At this stage, the associated wind pattern $\mathbf{q}_u{}^2$ indicates the presence of westerly anomalies over the equatorial west Pacific. The variance of the unfiltered monthly mean

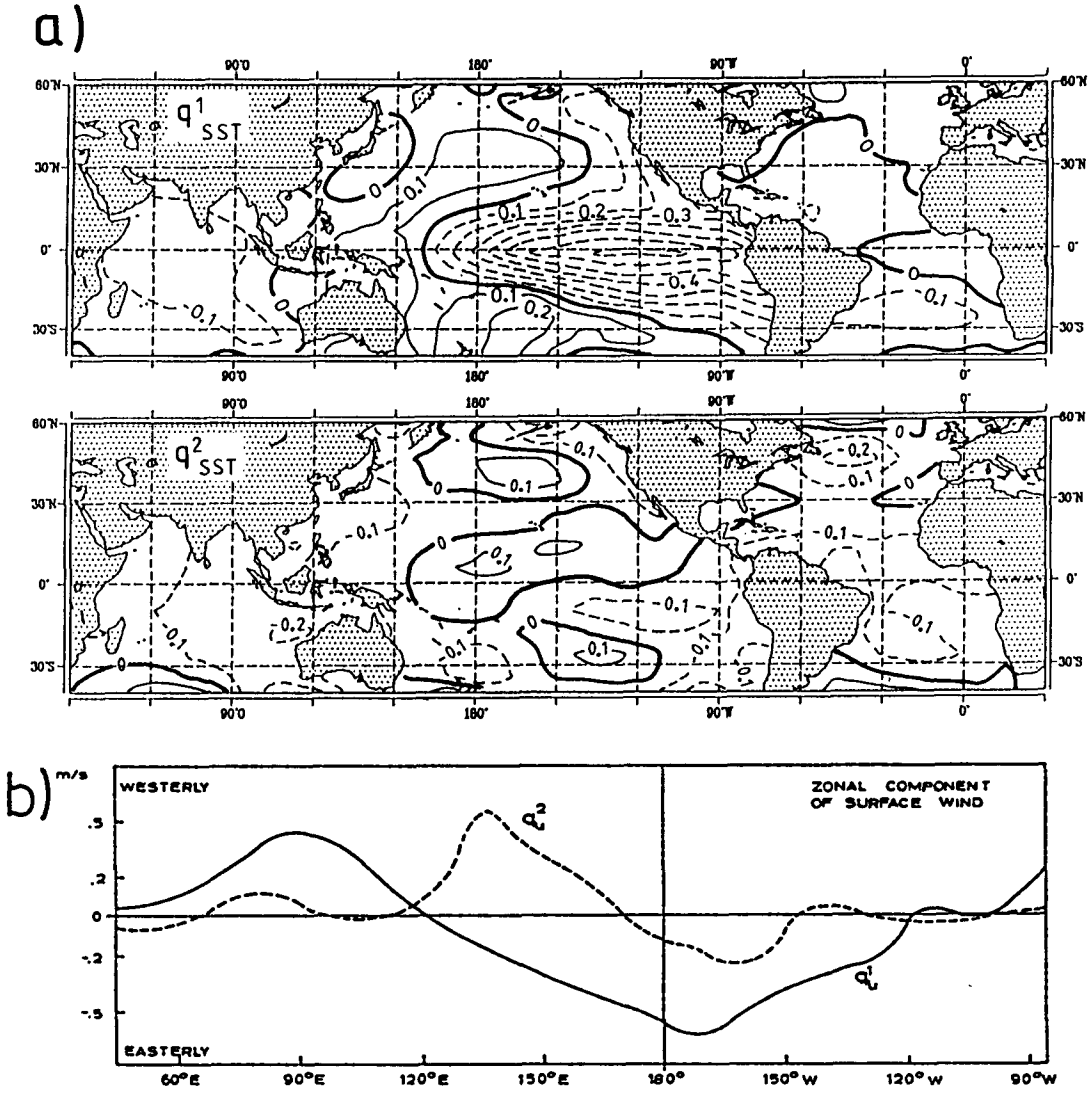

FIG. 3. Associated correlation patterns of (a) sea surface temperature, $\mathbf{q}^1_{sst}$ and $\mathbf{q}^2_{sst}$. Units: °C. (b) the zonal component of equatorial (45°E–85°W) surface wind, $\mathbf{q}_u{}^1$ and $\mathbf{q}_u{}^2$. Units: m s^{-1}. The associated $\mathbf{q}^1$ pattern tends to appear together with the SLP POP $\mathbf{P}^1$ pattern shown in Fig. 2, and the $\mathbf{q}^2$ pattern together with $\mathbf{P}^2$.

zonal wind explained by $\mathbf{q}_u^1$ and $\mathbf{q}_u^2$ is above 10% over the Indian Ocean and the western and central Pacific. (The relatively low levels of explained variance are a result of not filtering the analyzed data, so that the total variance contains a considerable amount of high-frequency variation.) Interestingly there is no signal over the equatorial east Pacific.

4. POP hindcast experiments

Using the POP pair identified in section 3, a POP prediction model is designed and tested in a series of hindcast experiments.

a. Design of the POP prediction model

The oscillation period T in (7) is not derived from the POP's eigenvalue but is taken from the cross-spectral analysis of the POP coefficient time series z^1 and z^2 and the SOI time series. Because z^1, $z^2(t)$, and the SOI exhibit maximum coherence at 30 months, $T = 30$ is chosen for all hindcast experiments. The time domain filter used to estimate the end points and the trajectory have approximately the same spectral characteristics as the spectral filter used in section 3 (see Appendix).

Hindcasts are made for each month from April 1974 to September 1988. The data from 1972 to March 1974 are disregarded because of too few observations to perform the filtering. Also, the data from the 1950s are not used because of data quality problems. This is illustrated by Fig. 1b, which shows the filtered SOI as derived from station data and from the gridded analyzed data. The deviation of the gridpoint time series from the station-based SOI is substantial in the fifties.

During the hindcast experiment period from 1974 to 1988, the Southern Oscillation is in a warm phase in 1976/77, 1982, and 1986/87; in a cold phase in 1975, 1981, and 1988; and in a quiet phase in 1978–80 and 1984–86. These ENSO phases could be hindcasted up to 12 months "in advance" throughout the period. The only exception was the 1975 cold phase, which was preceded by irregular conditions, namely the "aborted" 1974 El Niño (see below).

b. Case studies

In this subsection we show the hindcasts for three phases in some detail. These cases include both the best and the worst hindcast (warm event 1982/83 and cold event 1975/76). The results are displayed in the two-dimensional z-plane (Figs. 4–6). The two axes in the diagrams refer to the POP coefficients, z^1 and z^2; the solid (dashed) tilted line indicates the "El Niño" ("La Niña") direction defined by the phase between the POP coefficients and the SOI. The solid curve is the $\mathbf{z}$-trajectory, using the nonsymmetric filter (see Appendix), up to the time t_0. The hindcasts, prepared with the observations up to t_0, are indicated by the O-symbol.

The classification into "small", "normal," "very large events" follows (8). The $d(\mathbf{z})$ = constant contours are given by circles because the covariance matrix S is nearly a unit matrix. When the initial value, at t_0, lies outside the 33% circle and the analyzed trajectory propagates clockwise to the solid (dashed) line, a warm (cold) event is predicted to take place; when the trajectory departs from the solid (dashed) line a warm (cold) event is decaying; a trajectory within the "small" area indicates that no events will take place in the near future.

1) WARM EVENT 1982/83

Figure 4 shows the predicted evolutions using four initial times: t_0 = November 1981, and January, March, and May 1982. The analyzed POP coefficients evolve irregularly with small amplitude until northern spring 1981. In northern summer and fall of 1981 the coefficients are amplified and the trajectory begins to rotate clockwise, which indicates that the process described by the POP is "active." In November 1981 and in January 1982, a weak cold event is predicted to peak in January/February 1982, which might be followed by a weak warm event 14 months later (Figs. 4a and b). In March and May 1982 however, a dramatic intensification is monitored—the initial $\mathbf{z}$-values lie outside the 90% circle—and a very large warm event is predicted to peak in January 1983 (Figs. 4c and d).

2) COLD EVENT 1975/76

The prediction of the 1975 cold event is less satisfactory. This is demonstrated by Fig. 5 showing the hindcasts for November 1974 and July 1975. Because no data are available before April 1972, nonsymmetric filters had to be used to estimate the trajectory at its ends.

Having crossed the warm event line in summer 1972 and the cold event line one year later, the trajectory in early 1974 is entering the "quiet phase" stage; i.e., the inner 33% circle, indicting the breakdown of the process. Therefore the November 1974 hindcast is that no event will appear in 1975. A correct forecast could only have been made in July 1975; i.e., shortly before the cold event's peak phase, when the process is weakly reflected in the POPs (Fig. 5b).

3) QUIET PHASE 1985

The hindcasts using data up to September 1984 and January 1985 are shown in Fig. 6. In these hindcasts, the analyzed POP trajectory enters and stays within the 33% circle at the end of 1983. The system is correctly diagnosed as being in a quiet phase, and the prediction was that no event, cold or warm, was to be expected within the near future.

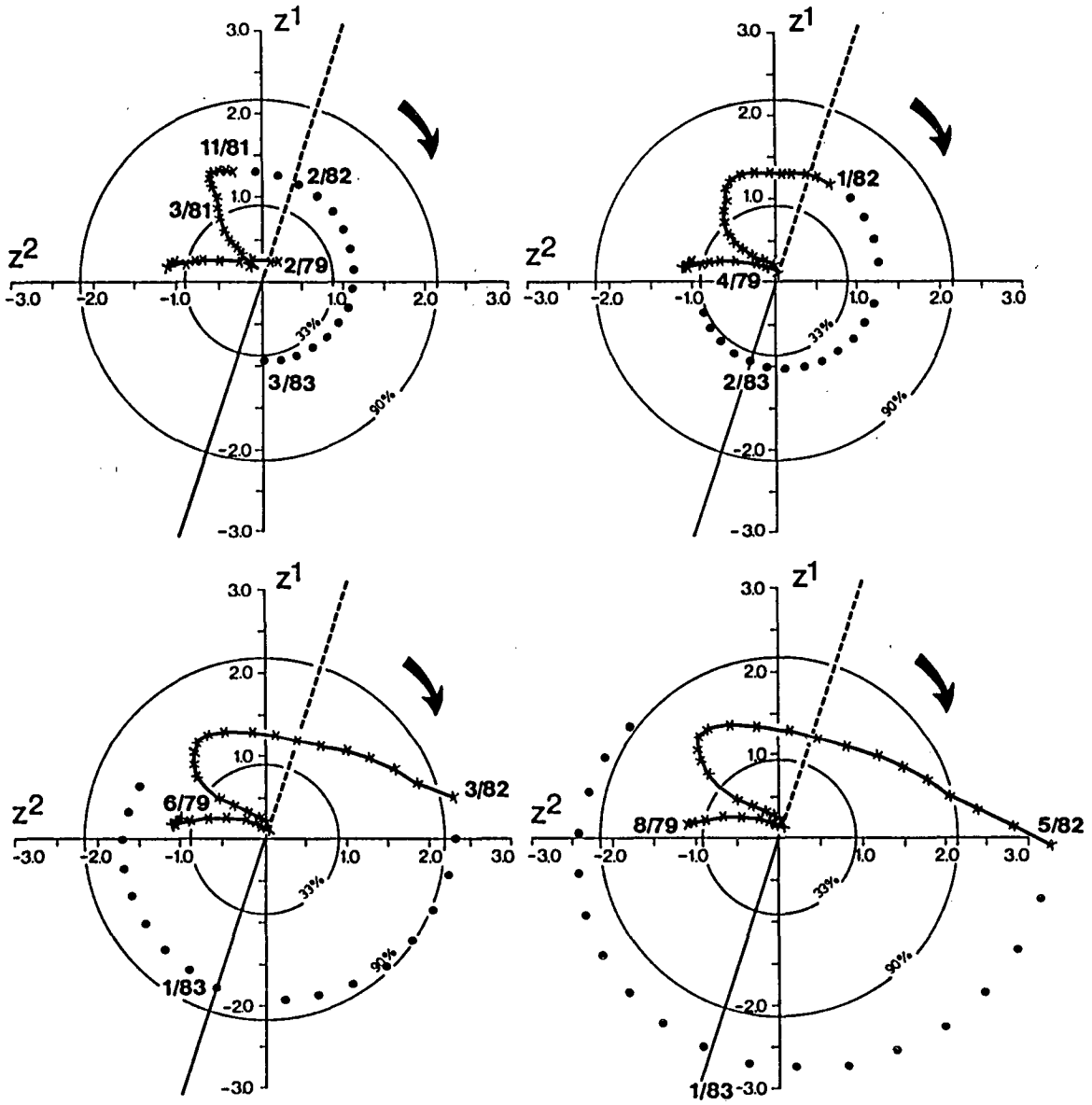

FIG. 4. Results for the hindcast experiments on the 1982 warm event displayed in the two-dimensional z-plane. Initial times t_0 = (a) November 1981, and (b) January, (c) March, and (d) May 1982. The two axes in the diagrams refer to the POP coefficients, z^1 and z^2; the solid (dashed) tilted line indicates the "El Niño" ("La Niña") direction defined by the phase between the POP coefficients and the SOI. The solid curve is the analyzed z-trajectory up to the time t_0. The hindcasts, prepared with the observations up to t_0, are indicated by the •-symbol. If the trajectory propagates clockwise to the solid (dashed) line, a warm (cold) event is predicted to take place. Similarly, moving off the El Niño/La Niña lines is interpreted as a decay of an event. A trajectory, which behaves irregularly or which is within the "small" area (given by the inner circle), indicates that no event will take place in near future. A trajectory outside the outer circle indicates the occurrence of a very large event.

c. *Hindcast skill of the POP model*

To assess the overall capability of the POP prediction scheme, a hindcast skill S^p is derived via (9) from all hindcast experiments. The low-pass filtered SOI (Fig. 1b) is used as the observed statistic $O(t)$. For the predictions, the statistic $P(t)$ is the predicted SOI.

The persistence forecast is used as a reference in order to assess the skill of the POP hindcasts. The unfiltered SOI is known to be affected by month-to-month variations that are not related to the state of the Southern Oscillation but that reflect, for example, the activity of the tropical 30–60 day wave. Therefore, the control forecast is based on 3-month running means, i.e.;

$$P_{\text{pers}}(t_0 + \tau) = P_{\text{pers}}(t_0) = \frac{\text{SOI}(t_0) + \text{SOI}(t_0 - 1) + \text{SOI}(t_0 - 2)}{3}. \quad (10)$$

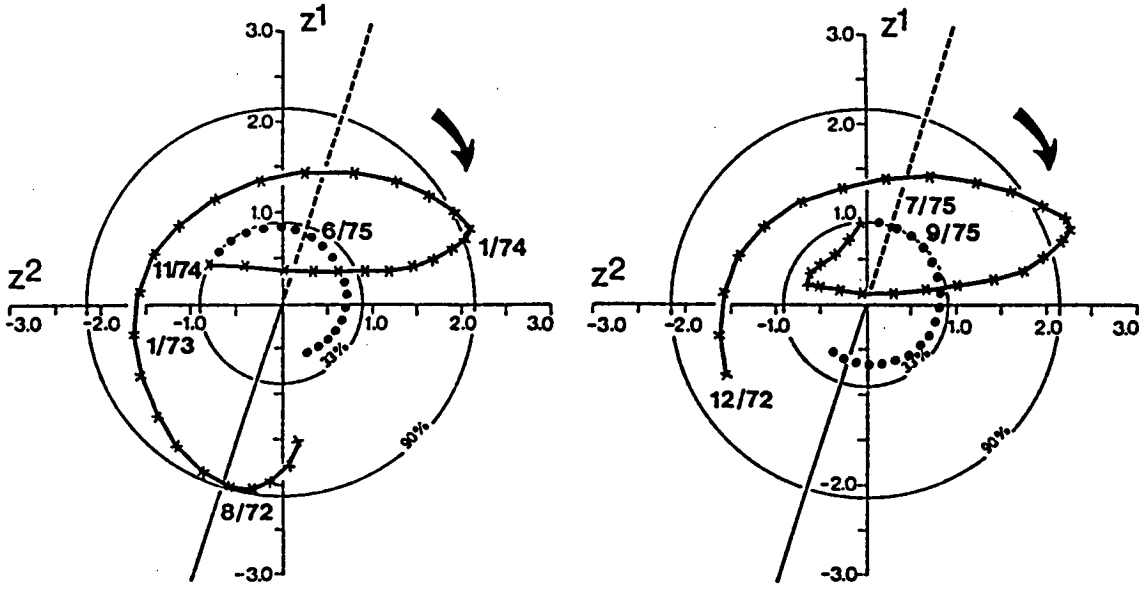

FIG. 5. Results for the hindcast experiments on the 1975 cold event. Initial times t_0 = November 1974 and July 1975. In winter 1975/76 the SOI is strongly positive. For description of the diagram, see caption to Fig. 4.

As a second reference forecast scheme we use the conventional ARMA (1,7;1) model derived from the monthly SOI by Chu and Katz (1985):

$$P_{\mathrm{ARMA}}(t+1) = 1.011 \cdot P(t) - 0.115 \cdot P(t-6) + \alpha_{t+1} - \theta_1 \alpha_t. \quad (11)$$

The white-noise forcing terms, α_{t+1} and $-\theta_1\alpha_t$, disregarded when performing the predictions.

The hindcast skill S^p at each time lag τ = 0–19 months, as calculated for the POP scheme for persistence according to (10) and for the ARMA model according to (11), is shown in Fig. 7. Persistence is clearly better for the "nowcast" and forecasts for lags $\tau \leq 2$ months. After that, the POP scheme is superior; after nine months, no correlation exists between persistence and observation, while the correlation between $P_{\mathrm{pop}}(t)$ and $O(t)$ is still about 40%. The ARMA model is

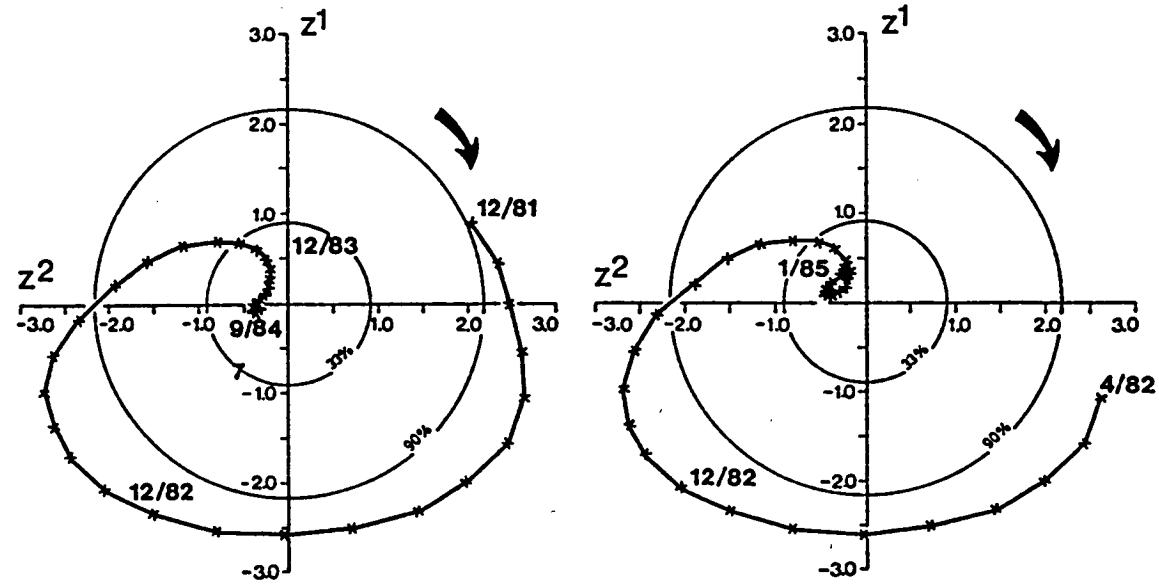

FIG. 6. Results for the hindcast experiments on the 1985 quiet phase. Initial times t_0 = September 1984 and January 1985. During 1984 and 1985, the SOI was small. For description of the diagram, see caption to Fig. 4.

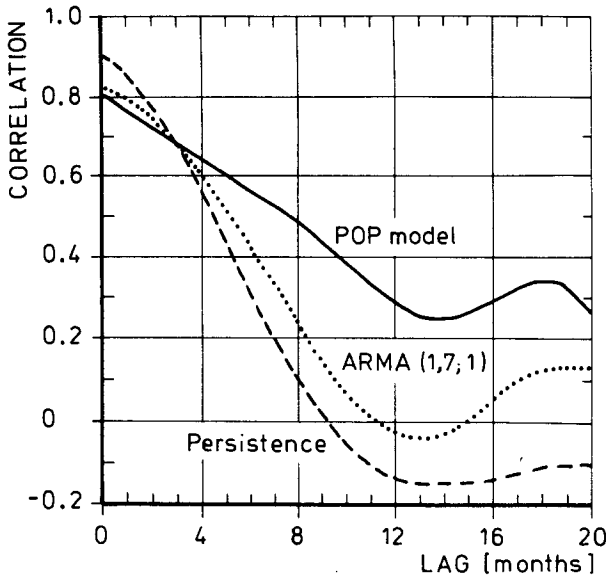

FIG. 7. Correlation skill S^p, according to (9), of the prediction of the southern oscillation index. Solid curve: POP prediction. Dashed curve: 3-month mean persistence. Dotted curve: ARMA(1;7,1) from Chu and Katz (1985).

somewhat better than the persistence but is clearly worse than the POP model.

The difference between the POP scheme and the ARMA model is that the former utilizes the full fields by projecting them onto a smaller set of dominant patterns. The POPs describe a propagating feature in the SLP field, whereas the ARMA describes the time evolution at one point only. The intervening state, $\mathbf{P}^2$, which plays an important role in the development of an ENSO event, cannot be described by the univariate SO index.

The fact that persistence is better than the POP scheme in the first months is expected. One reason is the nonsymmetric filtering to obtain initial values for the POP prediction. The second reason is the low-frequency variability of the SO, which is persistent on a time scale of a few months. The time scale of changes of the state of the SO is larger than one season ($T/4 \approx 8$ months), and it is here that the POPs are most successful in describing these changes.

It has to be kept in mind that the skill scores presented here are hindcast scores. If the time series were sufficiently long, one might derive the artificial skill by cross validation. For that purpose one would have to delete, for example, 2-yr episodes from the entire dataset, design a POP model with the remaining data, and calculate the skill for the 2-yr episode that would represent independent data.

In the present study, however, this is not possible because of the shortness of the time series and the necessity for low frequency filtering. If a 2-year interval were disregarded, a discontinuity at the ends of the interval would be introduced. This discontinuity would distort the time evolution for ± one year before and after the 2-yr interval (as mentioned in the Appendix) so that about four years of information would be lost for the POP analysis. In view of the limited reliability of the 1951–58 data, a loss of four years of data, in particular if events are included in this interval, is not acceptable for the POP analysis.

We believe, however, that the artificial skill is not substantial. As mentioned before, the POP forecast scheme is not strictly based on a least-square fit. Experiences in other studies, with sufficiently long time series, support this view (Storch and Xu 1990; Latif, personal communication). Also, the introduction of one-sided filtering in the prediction scheme reduces any artificial skill. A minor artificial skill might be introduced by inferring the oscillation period from the cross-spectral analysis of the POP coefficients and the SOI.

5. Discussion

a. The ENSO cycle

The POP analysis has identified a stochastic cyclic model of the Southern Oscillation

$$\ldots \rightarrow \mathbf{P}^1 \rightarrow \mathbf{P}^2 \rightarrow -\mathbf{P}^1 \rightarrow -\mathbf{P}^2 \rightarrow \mathbf{P}^1 \rightarrow \ldots$$

in which $\mathbf{P}^1$ describes the "peak phase" (Rasmusson and Carpenter 1982) of the SO when the Pacific SST anomalies were well developed. The $\mathbf{P}^2$ pattern represents an intermittent or "onset phase." It is dominated by a large SLP anomaly just east of the SPCZ area, which is associated with zonal wind anomalies in the west Pacific and generally weak SST anomalies. Such a cycle has been suggested earlier by van Loon and Shea (1985, 1987), who composited the Southern Hemisphere SLP field according to the state of the SO and the annual cycle. There are two major differences between our work and that of van Loon and Shea. First, our results were derived objectively without resort to any a priori information about the Southern Oscillation (except possibly the time scale); and second, the POP model is not locked to the annual cycle.

Additional data were used in order to test the reality of the proposed Southern Hemisphere ENSO cycle. Monthly mean SLP data from stations close to the anomaly centers of the $\mathbf{P}^1$ and $\mathbf{P}^2$ patterns were extracted from the World Meteorological Station Climatology data available at The National Center for Atmospheric Research. The strength of the $\mathbf{P}^1$ pattern may be approximated by the pressure difference between Darwin and Papeete; i.e., the traditional SOI, and the $\mathbf{P}^2$ pattern by the pressure in the center of the SPCZ region; (e.g., at Raoul Island) (position marked in Fig. 2). Two time series, the SOI and Raoul Island SLP, were subjected to cross-spectral analysis for the entire period 1951–82. SOI and Raoul SLP anomalies are highly coherent (squared coherence significant at

about the 99% level) and 90° out of phase on time scales of about 30–40 months. Consistent with this finding, Zwiers and Storch (1990) designed a nonlinear univariate "region dependent autoregressive" model in which the state of the SO is significantly controlled by the Southern Hemisphere circulation. Our result, and that of Zwiers and Storch, indicates that our finding of an ENSO cycle is not due to an artifact of the POP analysis technique.

Thus, the POP analysis leads to a concept of the Southern Oscillation that is fundamentally different from the traditional notion that the SO is a standing oscillation readily monitored by an index such as Darwin minus Papeete SLP. Instead, the POP model identifies the SO as a large-scale propagating atmospheric feature, which is insufficiently monitored by the SOI alone, as demonstrated by the low skill of the traditional ARMA scheme in Fig. 7. This result is in accord with some other studies of the SO; e.g., Barnett (1985, 1988), van Loon and Shea (1985, 1987), Gutzler and Harrison (1987), or Storch et al. (1989, 1990).

We suggest that the Southern Oscillation as a whole may be regarded as an oscillator with a basic time scale of about 2–3 years. The oscillator is modulated by random noise or possibly by some unknown forcing. As a result, the ENSO cycle exhibits variable "persistence" and the sequences of warm and cold events are of variable length.

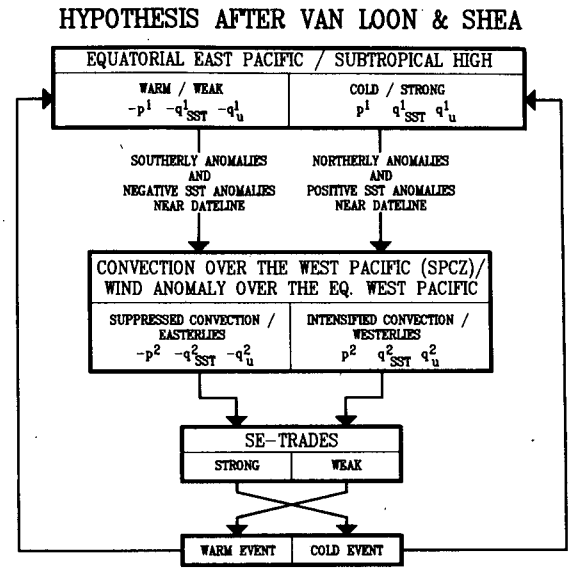

FIG. 8. van Loon and Shea's (1985, 1987) "SPCZ hypothesis" of the physics of the ENSO cycle.

b. *The role of the SPCZ*

The identification of strong anomalies in the strength of the SPCZ in the $\mathbf{P}^2$ pattern indicates that these anomalies might be essential in establishing the ENSO cycle. A hypothesis concerning the interaction between the SO and the SPCZ has been proposed by van Loon and Shea (1985, 1987) and Kiladis and van Loon (1988). This hypothesis is summarized in Fig. 8. During a cold event an anomalously strong subtropical high prevails in the east Pacific and negative SLP anomalies are located over the Indian Ocean and west Pacific. This SLP pattern is connected with northerly (warm) wind anomalies near the date line. These winds tend to cause positive SST anomalies in the area of the SPCZ, which is characterized by maximum convective activity throughout the year. Positive SST anomalies in such a region intensify the convective activity, causing below normal pressure (Storch et al. 1988). Consequently westerly wind anomalies appear over the equatorial west Pacific, which may trigger an El Niño event. This sign-reversed sequence of events will tend to initiate a cold event one year later.

The identification of anomalies in the SPCZ area that are connected with the Southern Oscillation does not *prove* that anomalies in that area cause the oscillation itself. It is equally possible that another process that is not resolved by our data might be responsible for the intervening stage of the SO. This unknown process might also cause the SPCZ anomalies. It may also be that the oscillator, identified by the POP analysis of Southern Hemisphere SLP, is just a part of a more complex system as suggested by Barnett (1985, 1988).

c. *Annual cycle and ENSO*

Many observational studies (e.g., Rasmusson and Carpenter 1982) suggest that ENSO is strongly locked to the annual cycle. Our analysis technique did not address the question of whether the POP model is phase-locked to the annual cycle. To answer this question we sorted the complex POP coefficient time series (Fig. 1a) $z(t)$ into eight classes: the complex plane is subdivided into eight regions, K_1, K_2, ... K_8. Each region is a 45° angular segment, so that all segments are of equal area. K_1 contains all active states with phase angles δ of $\frac{9}{8}\pi < \delta < \frac{7}{8}\pi$; K_2 is given by $\frac{7}{8}\pi < \delta < \frac{5}{8}\pi$; and so forth. Therefore, K_1 covers all states described by $-p^2$; K_2 states between $-p^2$ and p^1; K_3 p^1, etc.

A frequency table of $z(t)$ according to class and calendar month is given in Fig. 9. The number of samples available to estimate the frequencies is fairly small so that the results should be treated with caution. In spite of these limitations, however, Fig. 9 clearly demonstrates that the ENSO cycle, as described by the POP model, is locked to the annual cycle (as indicated by the tilted line). The intervening stages prior to an SO event—e.g., K_1/K_2 and K_4/K_5—tend to emerge in southern fall. The peak phases, $K_3 = p_1$ and $K_7 = -p_1$, are most frequent in southern winter and spring. Thus our analysis confirms the well-known result that the Southern Oscillation is linked to the annual cycle.

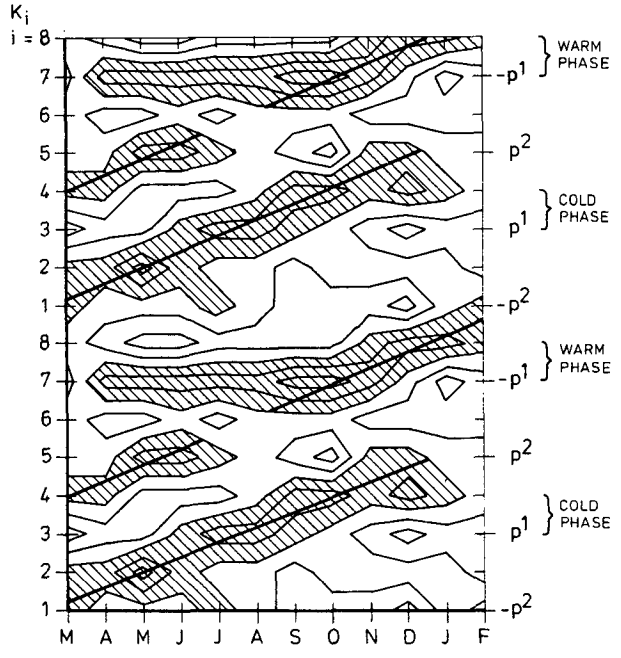

FIG. 9. Frequencies of the complex POP coefficients in class K_i (vertical axis) appearing in a calendar month (horizontal axis). To obtain a clearer picture the frequencies for two consecutive POP cycles are shown. For the detailed definition of the classes see text. Each of the 8 classes covers a 45° segment; the connection between classes and the appearance of the patterns p_1, $-p_1$, p_2 and $-p_2$ is indicated by the labels on the right. Contour interval is 1. Inside the hatched area, the frequencies are 3 and more.

d. *Predictions*

The concept of a natural oscillator, described by two patterns $\mathbf{P}^1$ and $\mathbf{P}^2$, offers a conceptually simple way to predict the state of the SO. The relevant point exploited in the prediction technique is the fact that the trajectory, defined by the POP coefficients in two-dimensional space, has some "inertia" and that future points of the trajectory may be deduced by simply prolonging the trajectory. Thus the POP prediction is deduced from "persistence of motion," in contrast to the "persistence of state" in a conventional persistence model. Therefore the POP prediction scheme is likely to be more successful in indicating the general evolution of the SO than in describing its details, such as anomalous SST averaged over certain areas. Also, the POP model is not able to predict a change from the "quiet phase" to the "active phase."

It was shown by the overall skill scores and case studies that POP prediction scheme may be able to forecast the state of the SO for two to three seasons in advance. One has to keep in mind, however, that all forecasts considered were made in the hindcast mode. Therefore it might be possible that the level of skill is in part contaminated by artificial skill.

For a lead time of more than one season the POP "persistence of motion" approach has a higher *hindcast* skill than the traditional "persistence of state" forecast. The scheme fails only one case, the cold event of 1975/76. In 1974/75, the ENSO process broke down (the "aborted" 1974/75 El Niño) but became reactivated in a relatively short time. Such behavior clearly cannot be described by the POP model, as was mentioned above.

Southern Oscillation predictions based on statistical models have been made by Barnett (1984) and Graham et al. (1987). Their approaches differ from ours with respect to both the predictors considered and the domain: tropical wind field (area averaged, Barnett 1984; or gridded, Graham et al. 1987) and global SLP (Graham et al. 1987). These approaches are also based on different hypotheses. The tropical wind models consider the equatorial waves generated by remote wind forcing; the global SLP model focuses on the eastward movement of Indo-Pacific SLP anomalies. In contrast, our model uses a nonequatorial predictor—Southern Hemisphere SLP between 15° and 40°S—and is based on the SPCZ hypothesis suggested by van Loon and Shea (1985, 1987). Interestingly, our predictions seem to have a skill that is comparable to that of the other stochastic schemes, in spite of the exclusion of the deep tropical area. This might be an indication that the oscillatory "Southern Oscillation" climate mode is not confined to the tropical region.

Acknowledgments. We with to express our gratitude to Harry van Loon and George Kiladis for their inspiration and technical help with the data, and to Klaus Hasselmann for his encouragement. We are indebted to Ben Santer who helped us with the English text, and to Mrs. Lewandowski, Marion Grunert, and Astrid v. Storch for carefully preparing the diagrams. We also with to thank BMRC for supplying us with the SLP analyses. The work was in part financed by the European Community Climate Program under Grant EV4C-0035-D(B).

APPENDIX

Time Filters in Frequency Domain and in Time Domain

A time series $\mathbf{x}(t)$ may be filtered in either the time domain or in the frequency domain. In the following we briefly summarize these two well-known concepts.

In the time domain the filter may be expressed as a linear operator

$$\tilde{\mathbf{x}}(t) = \sum_{j=-m}^{m} a_j \mathbf{x}(t + j\Delta t). \qquad \text{(A.1)}$$

If $\mathbf{x}(t)$ is a periodic function with the Fourier expansion

$$\mathbf{x}(t) = \sum_{\omega} \alpha(\omega) \exp(i\omega t)$$

the filtered time series is

$$\tilde{\mathbf{x}}(t) = \sum_{\omega} \alpha(\omega) \cdot G(\omega) \exp(i\omega t)$$

with

$$G(\omega) = \sum a_j \exp(i\omega j \Delta t). \qquad \text{(A.2)}$$

This way of calculating $\tilde{\mathbf{x}}$ is called *time domain filtering.* If the time domain filter is symmetric—i.e., $a_j = a_{-j}$—the amplitudes of the Fourier components are modified but the phases remain unchanged.

The same result, $\tilde{\mathbf{x}}$, may be obtained by deriving from the raw time series $\mathbf{x}$ the Fourier coefficients $\alpha(\omega)$, by multiplying the Fourier coefficients with the complex numbers $G(\omega)$ and by reconstructing the time series with the modified Fourier coefficients, $\alpha(\omega) \cdot G(\omega)$. This approach is called *frequency domain filtering.*

For each time domain filter there is an equivalent frequency domain filter, and frequency domain filters may be approximated by time domain filters.

In the present paper, filters are used on two different occasions to suppress non-SO related variability in the data. Prior to the POP analysis a frequency domain filter is applied with the filter characteristic:

$$G(\omega) = \begin{cases} 1, & 0 < \omega \leqslant \omega_2 \\ \frac{1}{2}\left\{1 - \cos\left[\dfrac{\pi}{\omega_1 - \omega_2}(\omega - \omega_1)\right]\right\}, & \omega_2 \leqslant \omega \leqslant \omega_1 \\ 0, & \omega > \omega_1 \end{cases}$$

with $\omega_1 = (15 \text{ months})^{-1}$ and $\omega_2 = (18 \text{ months})^{-1}$ (Fig. A1). A smooth change from "no change" ($0 < \omega \leqslant \omega_2$) to complete suppression ($\omega > \omega_1$) is introduced to avoid the generation of artificial secondary maxima due to "overshooting."

Because of the implicit assumption of periodicity, the filtered time series is distorted at its ends and also in the neighborhood of the break 1958/72. The distortion is limited to about ±1 year around the discontinuity.

The use of a filter is also necessary in preparing a POP forecast. Because future values are not available, a time domain filter has to be used. To obtain maximum consistency with the POP analysis, the frequency domain filter is approximated by a symmetric time domain filter with weights a_j. Because data are not available beyond the initial time, t_0, the filter has to be applied in a nonsymmetric mode:

$$\tilde{\mathbf{x}}(t_0 - k\Delta t) = \sum_{j=-m}^{k} a_j^* x(t_0 + (j-k)\Delta t)$$

with $a_j^* = a_j / \sum_{j=-m}^{k} a_j$. This normalization of the filter coefficients, $\sum a_j^* = 1$, is introduced to enforce $G(0) = 1$. That is, the filter does not change the mean. The lack of symmetry introduces phase errors that are, however, largest for high frequencies (see A.2). The phase error at a period of 30 months is about 1.5 months; for 40 months it is about 1 month.

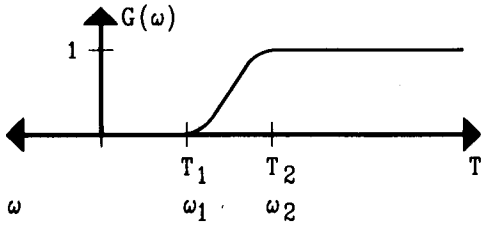

FIG. A1. Characteristic of the frequency domain filter used to suppress high-frequency variations. For details see text (Appendix).

REFERENCES

Barnett, T. P., 1984: Prediction of the El Niño 1982–83. *Mon. Wea. Rev.*, **112,** 1403–1407.

——, 1985: Variations in near-global sea level pressure. *J. Atmos. Sci.*, **42,** 478–501.

——, 1988: Variations in near-global sea level pressure: another view. *J. Climate,* **1,** 225–230.

——, N. Graham, M. Cane, S. Zebiak, S. Dolan, J. O'Brien and D. Legler, 1988: On the prediction of the El Niño of 1986–87. *Science,* **241,** 192–196.

——, L. Dümenil, U. Schlese, E. Roeckner and M. Latif, 1989: The effect of Eurasian snow cover on regional and global climate variations. *J. Atmos. Sci.*, **46,** 661–685.

Cane, M., and S. E. Zebiak, 1985: A theory for El Niño and the Southern Oscillation. *Science,* **228,** 1085–1087.

——, —— and S. C. Dolan, 1986: Experimental forecasts of El-Niño. *Nature,* **321,** 827–832.

Chu, P. S., and R. W. Katz, 1985: Modeling and forecasting the Southern Oscillation: A time-domain approach. *Mon. Wea. Rev.,* **113,** 1876–1888.

Gutzler, D. S., and D. E. Harrison, 1987: The structure and evolution of seasonal wind anomalies over the near-equatorial Eastern Indian and Western Pacific Oceans. *Mon. Wea. Rev.,* **115,** 169–192.

Graham, N. E., J. Michaelsen and T. P. Barnett, 1987: An investigation of the El Niño—Southern Oscillation cycle with statistical models. 2. Model Results. *J. Geophys. Res.,* **92,** 14271–14289.

Hasselmann, K., 1988: PIPs and POPs: the reduction of complex dynamical systems using Principal Interaction and Oscillation Patterns. *J. Geophys. Res.,* **93,** 11015–11021.

Inoue, M., and J. J. O'Brien, 1984: A forecasting model for the onset of El-Niño. *Mon. Wea. Rev.,* **112,** 2326–2337.

Kiladis, G. N., and H. van Loon, 1988: The Southern Oscillation. Part VII: Meteorological anomalies over the Indian and Pacific sectors associated with the extremes of the Oscillation. *Mon. Wea. Rev.,* **116,** 120–136.

Livezey, R., 1987: Caveat Emptor! The evaluation of skill in climate predictions. *Towards Understanding Climate Change,* V. Radok, Ed., Westview Press, 149–177.

Mo, K. C., and H. van Loon, 1985: Climate trends in the Southern Hemisphere. *J. Climate Appl. Meteor.,* **24,** 777–789.

Preisendorfer, R. W., 1988: *Principal Component Analysis in Meteorology and Oceanography.* Elsevier Science Publishers, 426 pp.

Rasmusson, E. M., and T. H. Carpenter, 1982: Variations in tropical sea surface temperature and surface wind fields associated with the Southern Oscillation/El Niño. *Mon. Wea. Rev.,* **110,** 354–384.

Ropelewski, C. F., and M. S. Halpert, 1987: Global and regional scale precipitation patterns associated with the El Niño/Southern Oscillation. *Mon. Wea. Rev.*, **115,** 1606–1626.

Suarez, M., and P. S. Schopf, 1988: A delayed action oscillator for ENSO. *J. Atmos. Sci.*, **45,** 3283–3287.

Storch, H. v., and J. Xu, 1990: Principal Oscillation Pattern analysis of the tropical 30 to 60 day oscillation. Part I: Definition of an index and its prediction. *Climate Dynamics,* in press.

——, H. van Loon and G. N. Kiladis, 1988: The Southern Oscillation: sensitivity to SST anomalies in the region of the South Pacific Convergence Zone. *J. Climate,* **1,** 325–331.

——, T. Bruns, I. Fischer-Bruns and K. H. Hasselmann, 1988: Principal Oscillation Pattern analysis of the 30 to 60 day oscillation in a GCM. *J. Geophys. Res.*, **93,** 11022–11036.

——, M. Latif and J. Biercamp, 1989: Simulation of the Southern Oscillation in an general circulation model. *Phil. Trans. Roy. Soc. London,* **A, 329,** 179–188.

——, U. Weese and J. Xu, 1990: Simultaneous analysis of space–time variability: Principal Oscillation Patterns and Principal Interaction Patterns with applications to the Southern Oscillation. *Z. Meteor.*, **40,** 99–103.

Trenberth, K. E., and D. J. Shea, 1987: On the evolution of the Southern Oscillation. *Mon. Wea. Rev.*, **115,** 3078–3096.

van Loon, H., 1984: The Southern Oscillation. Part III: Associations with the Trades and with the trough in the westerlies of the South Pacific Ocean. *Mon. Wea. Rev.*, **112,** 947–954.

——, and R. A. Madden, 1981: The Southern Oscillation. Part I: Global associations with pressure and temperature in northern winter. *Mon. Wea. Rev.*, **109,** 1150–1162.

——, and D. J. Shea, 1985: The Southern Oscillation. Part IV: The precursors south of 15°S to the extremes of the oscillation. *Mon. Wea. Rev.*, **113,** 2063–2074.

——, and K. Labitzke, 1987: The Southern Oscillation. Part V: The anomalies in the lower stratosphere of the Northern Hemisphere in winter and a comparison with the Quasi-biennial Oscillation. *Mon. Wea. Rev.*, **115,** 357–369.

——, and D. J. Shea, 1987: The Southern Oscillation. Part VI: Anomalies of sea level pressure on the Southern Hemisphere and of Pacific sea surface temperature during the development of a Warm Event. *Mon. Wea. Rev.*, **115,** 370–379.

White, W. B., S. E. Pazan and M. Inoue, 1987: Hindcast/forecast of ENSO events based on the redistribution of observed and model heat content in the western tropical Pacific. *J. Phys. Oceanogr.*, **17,** 264–280.

Wright, P. B., 1984: Relationships between indices of the Southern Oscillation. *Mon. Wea. Rev.*, **112,** 1913–1919.

Zwiers, F., and H. von Storch, 1990: Region dependent auto-regressive time series modeling of the Southern Oscillation. *J. Climate,* **3,** 1347–1363.